

# Economic Operation of Droop-Controlled AC Microgrids

Rabih A. Jabr , Fellow, IEEE

**Abstract**—Linear droop control is a standard approach for the decentralized operation of AC microgrids. While the traditional design of the real and reactive power droop functions does not consider economic aspects, recent approaches present modifications to enable least-cost operation. This paper proposes mixed-integer conic programming (MICP) for computing the real and reactive power droop parameters from a stochastic optimization framework that captures several snapshots of the microgrid's operation. The model permits distributed generation to switch between grid-forming and grid-feeding modes. Unlike previous works, MICP provides droop parameters that are globally optimal for the design scenarios. Numerical results show that using traditional linear cost-based droop design methods may result in voltage magnitude violations. In contrast, the proposed method gives a solution free of violations and is yet more economical.

**Index Terms**—AC microgrids, droop control, economic dispatch, optimization methods, power-sharing, voltage control.

## NOMENCLATURE

$\alpha_i^k / \beta_i^k$	Binary variable denoting the choice of the $k^{th}$ real/reactive power droop gain from a discrete set.
$c_{gj}^k$	Slope of the piecewise linear cost function of generator $j$ over the $k^{th}$ segment.
$C_j(P_{gj})$	Cost function of generator $j$ evaluated at $P_{gj}$ .
$E$	Set of branches.
$\eta_{P_i}^{(k,s)} / \eta_{Q_i}^{(k,s)}$	Binary variable associated with the real/reactive power big-M constraints of generator $i$ over the $k^{th}$ choice of droop gain during scenario $s$ .
$f$	System frequency.
$f_{0i}$	No-load frequency setpoint of generator $i$ .
$\underline{\gamma}_i^{(s)} / \underline{\lambda}_i^{(s)}$	Binary variable denoting generator's $i$ operation at the lower real/reactive power dispatch limit during scenario $s$ .
$\bar{\gamma}_i^{(s)} / \bar{\lambda}_i^{(s)}$	Binary variable denoting generator's $i$ operation at the upper real/reactive power dispatch limit during scenario $s$ .
$g_j / b_j$	Shunt conductance/susceptance at node $j$ .

Manuscript received July 30, 2021; revised October 17, 2021; accepted November 20, 2021. Date of publication November 23, 2021; date of current version June 20, 2022.

The author is with the Department of Electrical and Computer Engineering, American University of Beirut, Beirut 1107 2020, Lebanon (e-mail: rabih.jabr@aub.edu.lb).

Color versions of one or more figures in this article are available at <https://doi.org/10.1109/TPWRS.2021.3130128>.

Digital Object Identifier 10.1109/TPWRS.2021.3130128

$K_{i,max}'' / K_{i,av}''$	Correction factor of generator $i$ in the maximum/average cost-based scheme.
$K_{P_i} / K_{Q_i}$	Real/reactive power droop gain of generator $i$ .
$K_{P_i}^{(k)} / K_{Q_i}^{(k)}$	$k^{th}$ choice of the real/reactive power droop gain of generator $i$ .
$K_{P_i}^{ac} / K_{Q_i}^{ac}$	Average cost-based real/reactive power droop gain of generator $i$ .
$K_{P_i}^{mc} / K_{Q_i}^{mc}$	Maximum cost-based real/reactive power droop gain of generator $i$ .
$K_{P_i}^{tr} / K_{Q_i}^{tr}$	Traditional real/reactive power droop gain of generator $i$ .
$K_{Q_{ci}}^{(k)}$	$k^{th}$ choice of the reactive power droop gain of generator $i$ in the function of the squared voltage magnitude.
$\ell_{ij}$	Squared current magnitude in the branch $ij$ .
$M_{P_i}^{(k)-} / M_{Q_i}^{(k)-}$	Lower real/reactive power big-M parameter for generator $i$ at the $k^{th}$ choice of droop gain.
$M_{P_i}^{(k)+} / M_{Q_i}^{(k)+}$	Upper real/reactive power big-M parameter for generator $i$ at the $k^{th}$ choice of droop gain.
$n$	Number of nodes.
$n_c$	Number of piecewise linear segments in the cost function.
$n_d$	Number of droop gain choices in a discrete set.
$n_g$	Number of generators.
$n_s$	Number of scenarios.
$\nu_{0i}$	No-load squared voltage magnitude setpoint of generator $i$ .
$\nu_i$	Squared voltage magnitude at node $i$ .
$P_{di} / Q_{di}$	Real/reactive power demand at node $i$ .
$P_{gi} / Q_{gi}$	Real/reactive power of generator $i$ .
$P_{gi}^{d(s)} / Q_{gi}^{d(s)}$	Real/reactive power of generator $i$ in its dispatch range during scenario $s$ .
$P_{gj}^{(k)}$	Real power of generator $j$ at the $k^{th}$ breakpoint.
$P_{gj}^k$	Real power of generator $j$ in the $k^{th}$ segment.
$P_{ij} / Q_{ij}$	Real/reactive power flow in the branch $ij$ .
$P_j / Q_j$	Real/reactive power injection at node $j$ .
$\rho^{(s)}$	Probability of occurrence of scenario $s$ .
$r_{ij} / x_{ij}$	Resistance/reactance of branch $ij$ .
$V_{0i}$	No-load voltage magnitude setpoint of generator $i$ .
$V_i$	Voltage magnitude at node $i$ .
• min/max	Minimum/maximum value of a quantity.
• (s)	Value of a quantity in scenario $s$ .

## I. INTRODUCTION

**T**HE increased integration of distributed generators in distribution grids has propelled the evolution of microgrids that can operate in grid-connected or islanded modes. The control of microgrids is generally hierarchical and comprises three control levels as described in [1]. In islanded AC microgrid operation, which is the central theme of this work, two control levels are applicable: primary control and secondary control [2]. The primary control is classical droop control for synchronous generators and has been adapted to inverter-based distributed generators. It aims to divide the load demand amongst the distributed generators in proportion to their power ratings [3]. Classical droop control inherently assumes that the line has a high inductive reactance to resistance ratio, typical of high-voltage AC networks. Nonetheless, droop control is still applicable in low and medium-voltage AC microgrids with the help of the virtual impedance [4]. As the load varies, primary control allows the distributed generators to share the power autonomously but giving rise to steady-state frequency and voltage deviations. Secondary control restores the frequency and voltage deviations while dispatching the energy sources economically.

The secondary control is ideally centralized and achieves very economical operation, but it commands extensive communication requirements and needs high-performance computation to manage large amounts of data [5], [6]. Additionally, centralized secondary control raises reliability concerns linked with single-point failures [4]. Therefore, the consensus algorithm has been proposed as a solution to overcome the shortcoming of centralized control. The consensus algorithm is implemented via distributed control, which is surveyed in [7]. It aims to achieve agreement on a data value amongst distributed systems, in this case, the distributed generators and the processes controlling them. For economic dispatch, an ideal choice for the data value that the generators need to agree on is the incremental system cost in the well-known equal-lambda criterion [8], [9]; the formulation can include transmission losses [10] and power dispatch limits [11]. Unfortunately, the distributed consensus methods rely upon each generator knowing the system power mismatch, which remains a challenge for totally distributed systems. However, a promising solution that combines both the consensus protocol and frequency control has been recently reported in [12]. Furthermore, the accuracy of the consensus algorithm is also dependent on data exchange via a communication network, although such a network is not as extensive as in the centralized case. Ref. [13] proposed a compartmentalization strategy to simplify the communication structure further and reduce the dependency on communication networks, and [14] discussed including demand response within the distributed optimization for economic dispatch.

At the other extreme, economic dispatch-based decentralized control strategies do not require a communication infrastructure. Instead of having the least cost operations entirely relegated to centralized or distributed secondary control, it is possible to include the generation economics into primary generation control through modifying the droop control law. There are different modification strategies for the nonlinear droop curves: in the

function of the incremental cost [15]–[17], based on the relative values of generation cost [18], or a combination of integer and fractional power functions whose parameters are obtained by an optimization heuristic [19]. The real and reactive power droop modification method in [20] is also based on the relative cost function values. Still, it gives rise to simple linear characteristics with the plug-and-play flexibility of existing implementations maintained.

This work proposes a stochastic optimization framework to compute active and reactive linear droop curve parameters, i.e., the no-load setpoint and droop gain, while considering the operational economics of units with practical nonlinear convex cost curves, as reported for example in [18], [20]. Although the droop curves are linear to maintain compatibility with the classical droop implementation, the no-load setpoints and droop gains are computed from a mixed-integer conic programming formulation that can provide optimality guarantees for the combination of chosen system snapshots. Such assurances are not available from the above surveyed decentralized methods. Furthermore, the proposed framework considers a conic network model for each snapshot representing a decentralized operation [21], thus alleviating potential voltage magnitude violation problems that may appear under droop control. Finally, the distributed generators are modeled via grid-forming or grid-feeding modes, depending on the operating region [22]–[24]. Out-of-sample analysis shows performance very close to what can be anticipated from a fully centralized operation. Recent work has also demonstrated the effectiveness of mixed-integer convex programming design in the context of DC microgrids [25].

This paper focuses on designing the real and reactive power linear droop control laws, a simple and practical format of droop control. The article is the first to propose a formulation that provides a globally optimal solution for a predefined set of scenarios; this is the paper's main contribution. The originality is in setting the control parameters in a way much better than existing techniques and yet remaining compatible with the current hardware implementations. The rest of this paper is organized as follows. Section II reviews the classical linear droop control paradigm with some modifications for cost-based dispatch [20]. Then, Section III presents the stochastic optimization framework for droop controller design via mixed-integer conic programming. Numerical results are given in Section IV and contrast the effectiveness of the proposed controller designs with those from Section II, in addition to a globally optimal centralized solution [26]. Finally, the paper is concluded in Section V. The Appendix includes the details of power flow implementation with droop control, as it is required in the comparative analysis.

## II. DROOP CONTROL

Distributed generators in a microgrid commonly adopt linear droop control for sharing the real and reactive power loading. This section discusses the classical scheme for choosing the parameters of the droop straight-line relationships and a recent modification geared towards the economic operation. The distributed generators are connected at nodes 1 to  $n_g$  and are referred to below by their connection node number. Each

generator has a convex cost function  $C_i(P_{gi})$ , whose general format is given in [20], and where  $P_{gi}$  is the generated real power.

### A. Traditional Linear Droop Scheme

The traditional linear droop method allows the generators to share their real and reactive power in proportion to their power ratings [3], [20]. Eq (1) is the real power linear droop equation depicting how the system frequency drops gradually with the actual real power generation  $P_{gi}$ . Two parameters define the real power linear droop equation:  $f^{\max}$ , the maximum frequency, and  $K_{P_i}^{tr}$ , the real power droop gain computed in (2). In (2),  $f^{\min}$  is the minimum frequency, and  $P_{gi}^{\max}$  is the rated real power generation. Similarly, (3) is the reactive power droop equation, and (4) is the reactive power droop gain. In (3) and (4),  $V_i$  is the voltage magnitude of the generator connected at node  $i$ ,  $V_i^{\min}$  and  $V_i^{\max}$  are the minimum and maximum values,  $Q_{gi}$  is the actual reactive power generation, and  $Q_{gi}^{\max}$  is the rated reactive power value.

$$f = f^{\max} - K_{P_i}^{tr} P_{gi}, \quad i = 1, \dots, n_g \quad (1)$$

$$K_{P_i}^{tr} = \frac{f^{\max} - f^{\min}}{P_{gi}^{\max}} \quad (2)$$

$$V_i = V_i^{\max} - K_{Q_i}^{tr} Q_{gi}, \quad i = 1, \dots, n_g \quad (3)$$

$$K_{Q_i}^{tr} = \frac{V_i^{\max} - V_i^{\min}}{Q_{gi}^{\max}} \quad (4)$$

### B. Cost-Based Linear Droop Schemes

Ref. [20] modified the real and reactive power droop gains so that the generators economically share the load power. Two schemes are proposed: the first is based on the full-load generation cost and the second on the average generation cost.

1) *Maximum Cost-Based Scheme*: The maximum cost ( $mc$ ) scheme for droop control ((5) and (7)) employs the power droop gains given by (6) and (8). The droop gains in the maximum cost-based scheme are formed by the traditional droop gains multiplied by a correction factor  $K_{i,\max}''$  for each generator- $i$ . Ref. [20] defines the correction factor in (9), where  $C_{i,\max}''$  is the full-load cost of the generator- $i$  minus the no-load cost, all normalized by the maximum power rating. The rationale behind the choice of the correction factors is that the least costly generators must contribute most of the load power.

$$f = f^{\max} - K_{P_i}^{mc} P_{gi}, \quad i = 1, \dots, n_g \quad (5)$$

$$K_{P_i}^{mc} = K_{P_i}^{tr} K_{i,\max}'' \quad (6)$$

$$V_i = V_i^{\max} - K_{Q_i}^{mc} Q_{gi}, \quad i = 1, \dots, n_g \quad (7)$$

$$K_{Q_i}^{mc} = K_{Q_i}^{tr} K_{i,\max}'' \quad (8)$$

$$K_{i,\max}'' = \frac{C_{i,\max}''}{\max(C_{1,\max}'', \dots, C_{i,\max}'', \dots, C_{n_g,\max}'')} \quad (9)$$

2) *Average Cost-Based Scheme*: The average cost ( $ac$ ) scheme is similar to the one above, except for the generator

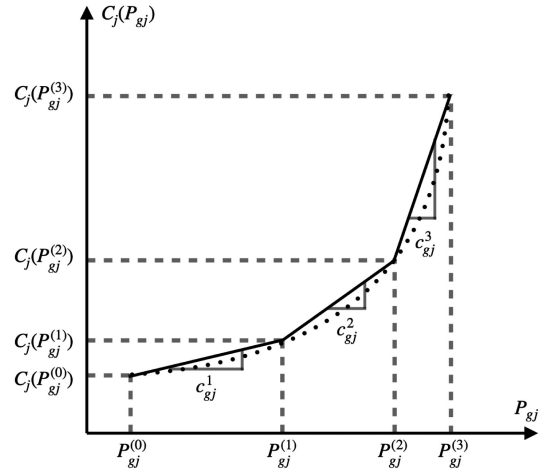


Fig. 1. Piecewise linear cost curve with  $n_c = 3$ .

correction factors (12) used in calculating the droop gains (10) and (11).  $C_{i,\text{av}}''$  in (12) uses the average cost of generator- $i$  instead of the full-load cost as in (9).

$$K_{P_i}^{ac} = K_{P_i}^{tr} K_{i,\text{av}}'' \quad (10)$$

$$K_{Q_i}^{ac} = K_{Q_i}^{tr} K_{i,\text{av}}'' \quad (11)$$

$$K_{i,\text{av}}'' = \frac{C_{i,\text{av}}''}{\max(C_{1,\text{av}}'', \dots, C_{i,\text{av}}'', \dots, C_{n_g,\text{av}}'')} \quad (12)$$

### III. MIXED-INTEGER CONIC PROGRAMMING FOR DROOP CONTROL DESIGN

The cost-based schemes described above reduce the operational cost as compared to the traditional droop control [20]. The straight-line parameters (no-load setpoint and droop gain) in subsection II-B are heuristically obtained, and therefore their computation using formal optimization theory is expected to give lower operational costs. Additionally, the heuristic tuning of the droop gains does not account for the microgrid network model, thus permitting voltage magnitude violations during droop control. This section proposes a mixed-integer conic programming (MICP) formulation for designing the droop controllers; the formulation employs several snapshots of the system represented via its conic network model in a stochastic optimization framework.

A piecewise linear formulation (13)–(16) can approximate the distributed generator convex cost curves as given in [20]. In the approximation, the cost curve is represented by  $n_c$  linear segments interpolating between  $n_c + 1$  breakpoints:  $(P_{gj}^{(0)}, C_j(P_{gj}^{(0)}))$ ,  $\dots$ ,  $(P_{gj}^{(k)}, C_j(P_{gj}^{(k)}))$ ,  $\dots$ ,  $(P_{gj}^{(n_c)}, C_j(P_{gj}^{(n_c)}))$ ; Fig. 1 shows an illustration for  $n_c = 3$ . The abscissa of the first point  $P_{gj}^{(0)}$  is the same as the minimum generation  $P_{gj}^{\min}$ , and the last point,  $P_{gj}^{(n_c)}$ , coincides with the maximum generation  $P_{gj}^{\max}$ . Eq (16) gives the slope of each interpolating segment.

$$C_j(P_{gj}) = C_j(P_{gj}^{(0)}) + \sum_{k=1}^{n_c} c_{gj}^k P_{gj}^k, \quad j = 1, \dots, n_g \quad (13)$$

$$P_{gj} = P_{gj}^{(0)} + \sum_{k=1}^{n_c} P_{gj}^k \quad (14)$$

$$0 \leq P_{gj}^k \leq P_{gj}^{(k)} - P_{gj}^{(k-1)}, j = 1, \dots, n_g, k = 1, \dots, n_c \quad (15)$$

$$c_{gj}^k = \frac{C_j(P_{gj}^{(k)}) - C_j(P_{gj}^{(k-1)})}{P_{gj}^{(k)} - P_{gj}^{(k-1)}} \quad (16)$$

$$j = 1, \dots, n_g, k = 1, \dots, n_c$$

### A. Conic Network Model

The conic network model is a relaxation applicable to radial networks that allows recovering global solutions of some optimal power flow (OPF)-type problems. The conic network model was first proposed using the bus injection relaxation [27] and later using the branch flow relaxation [26]. The conic model adopted herein employs the branch flow relaxation as it avoids subtracting variables with similar values, thus giving better numerical computing characteristics [28]. The minimum cost branch flow conic OPF [21] is given by (17)–(26):

$$\min \sum_{j=1}^{n_g} C_j(P_{gj}) \quad (17)$$

$$P_j = \sum_{k:j \rightarrow k} P_{jk} - \sum_{i:i \rightarrow j} (P_{ij} - r_{ij}\ell_{ij}) + g_j\nu_j, j = 1, \dots, n \quad (18)$$

$$Q_j = \sum_{k:j \rightarrow k} Q_{jk} - \sum_{i:i \rightarrow j} (Q_{ij} - x_{ij}\ell_{ij}) + b_j\nu_j, j = 1, \dots, n \quad (19)$$

$$\nu_j = \nu_i - 2(r_{ij}P_{ij} + x_{ij}Q_{ij}) + (r_{ij}^2 + x_{ij}^2)\ell_{ij}, \forall (i, j) \in E \quad (20)$$

$$\nu_i\ell_{ij} \geq P_{ij}^2 + Q_{ij}^2, \forall (i, j) \in E \quad (21)$$

$$P_j = \begin{cases} P_{gj} - P_{dj}, & j = 1, \dots, n_g \\ -P_{dj}, & j = n_g + 1, \dots, n \end{cases} \quad (22)$$

$$Q_j = \begin{cases} Q_{gj} - Q_{dj}, & j = 1, \dots, n_g \\ -Q_{dj}, & j = n_g + 1, \dots, n \end{cases} \quad (23)$$

$$Q_{gj}^{\min} \leq Q_{gj} \leq Q_{gj}^{\max}, j = 1, \dots, n_g \quad (24)$$

$$\nu_i^{\min} \leq \nu_i \leq \nu_i^{\max}, i = 1, \dots, n \quad (25)$$

$$\ell_{ij}^{\min} \leq \ell_{ij} \leq \ell_{ij}^{\max}, \forall (i, j) \in E \quad (26)$$

where:

- $n$  is the number of nodes,
- $E$  is the set of branches,
- $r_{ij}/x_{ij}$  is the resistance/reactance of branch  $ij$ ,
- $g_j/b_j$  is the shunt conductance/susceptance at node  $j$ ,
- $P_j/Q_j$  is the real/reactive power injection at node  $j$ ,
- $P_{ij}/Q_{ij}$  is the real/reactive power flow in the branch  $ij$ ,
- $\ell_{ij}$  is the squared current magnitude in the branch  $ij$ , and
- $\nu_i$  is the squared voltage magnitude at node  $i$ .

Eqs. (22)–(23) distinguish between power injections at load (subscript  $d$ ) and generation (subscript  $g$ ) nodes, and (24)–(26) impose operational min/max limits on reactive power generation  $Q_{gi}$ , squared voltage magnitude  $\nu_i$ , and squared branch current  $\ell_{ij}$ . The limits on real power generation are implicitly implied through the piecewise linear cost equations (14)–(15).

The following vectors are introduced to simplify the presentation in the remainder of this paper:

- $\ell_b = [\ell_{ij} : (i, j) \in E]$
- $P_b = [P_{ij} : (i, j) \in E]$ ,  $Q_b = [Q_{ij} : (i, j) \in E]$
- $P_d = [P_{di} : i = 1, \dots, n]$ ,  $Q_d = [Q_{di} : i = 1, \dots, n]$
- $P_g = [P_{gi} : i = 1, \dots, n_g]$ ,  $Q_g = [Q_{gi} : i = 1, \dots, n_g]$
- $\nu = [\nu_i : i = 1, \dots, n]$

The conic OPF problem given by (17)–(26) and (13)–(15) can then be placed in the compact form below, where  $P_d$  and  $Q_d$  are input parameter vectors to the optimization problem, and the remaining vectors are computed from the optimization problem.

$$\min C(P_g) \quad (27)$$

$$F(\ell_b, P_b, P_d, P_g, Q_b, Q_d, Q_g, \nu) \leq 0 \quad (28)$$

### B. Conic Programming-Based Droop Design Scheme

The conic OPF (27)–(28) forms the basis of computing the real and reactive power droop relationship parameters using a stochastic optimization formulation. Consider  $n_s$  snapshots of the network that include different load scenarios and possible contributions from non-dispatchable distributed generators modeled as negative loads. The load scenarios and contributions from non-dispatchable distributed generators are in practice obtained from historical observations. Let  $\rho^{(s)}$  denote the probability of occurrence of a particular scenario. The conic programming-based stochastic optimization formulation minimizes the expected cost of operation given by (29), subject to the network and operational constraints in each scenario (30), the scenario frequency being between its limits (31), and the droop control rules that couple the manner of real and reactive power dispatch across the various scenarios as discussed in III-B1–III-B2.

$$\min \sum_{s=1}^{n_s} \rho^{(s)} C(P_g^{(s)}) \quad (29)$$

$$F(\ell_b^{(s)}, P_b^{(s)}, P_d^{(s)}, P_g^{(s)}, Q_b^{(s)}, Q_d^{(s)}, Q_g^{(s)}, \nu^{(s)}) \leq 0 \quad s = 1, \dots, n_s \quad (30)$$

$$f^{\min} \leq f^{(s)} \leq f^{\max}, s = 1, \dots, n_s \quad (31)$$

1) *Real Power Droop*: The real power generation  $P_{gi}^{(s)}$  in a given scenario is given by (32), where the real power droop equation is  $f^{(s)} = f_{0i} - K_{Pi}P_{gi}^{(s)}$ . When  $P_{gi}^{(s)}$  is at the minimum generation value  $P_{gi}^{\min}$ , the scenario frequency  $f^{(s)}$  is greater than or equal to the maximum frequency given by the droop relationship. Similarly, when  $P_{gi}^{(s)}$  is at the maximum generation value  $P_{gi}^{\max}$ ,  $f^{(s)}$  is less than or equal to the minimum frequency value of the droop relationship. Other than the extreme limits,

$P_{gi}^{(s)}$  can be equal to  $P_{gi}^{d(s)}$ , which is related to the scenario frequency using the real power droop equation. Note that operation at the limits is consistent with the grid-feeding mode, whereas the droop relation applies to grid-forming [22]–[24].

$$P_{gi}^{(s)} = \begin{cases} P_{gi}^{\min}, & f^{(s)} \geq f_{0i} - K_{Pi} P_{gi}^{\min} \\ P_{gi}^{d(s)}, & f^{(s)} = f_{0i} - K_{Pi} P_{gi}^{d(s)} \\ P_{gi}^{\max}, & f^{(s)} \leq f_{0i} - K_{Pi} P_{gi}^{\max} \end{cases}$$

$$i = 1, \dots, n_g, s = 1, \dots, n_s \quad (32)$$

$$P_{gi}^{\min} \leq P_{gi}^{(s)} \leq P_{gi}^{\max}, i = 1, \dots, n_g, s = 1, \dots, n_s \quad (33)$$

The optimization solution gives the optimal choice of the linear droop parameters, i.e.,  $f_{0i}$  that varies in a continuous range (34), and the droop gain  $K_{Pi}$  that can take values from a discrete set (35). A discrete set allows turning the problem into a mixed-integer conic program by avoiding the bilinear terms in the middle equation of (32), as described in subsection III-C. However, if any of the droop gains is represented as a continuous variable, its bilinear term will give rise to a non-convex continuous relaxation, making it impossible to use MICP to achieve a global solution.

$$f_{0i}^{\min} \leq f_{0i} \leq f_{0i}^{\max}, i = 1, \dots, n_g \quad (34)$$

$$K_{Pi} \in \left\{ K_{Pi}^{(1)}, \dots, K_{Pi}^{(n_d)} \right\}, i = 1, \dots, n_g \quad (35)$$

2) *Reactive Power Droop*: Eqs. (36)–(39) for the reactive power droop parallel the presentation of (32)–(35) for the real power droop. Thus, in a given scenario, the reactive power generation  $Q_{gi}^{(s)}$  can be at the minimum value  $Q_{gi}^{\min}$ , the maximum value  $Q_{gi}^{\max}$ , or at a value  $Q_{gi}^{d(s)}$  governed by the reactive power droop equation  $\nu_i^{(s)} = \nu_{0i} - K_{Qci} Q_{gi}^{d(s)}$ .

$$Q_{gi}^{(s)} = \begin{cases} Q_{gi}^{\min}, & \nu_i^{(s)} \geq \nu_{0i} - K_{Qci} Q_{gi}^{\min} \\ Q_{gi}^{d(s)}, & \nu_i^{(s)} = \nu_{0i} - K_{Qci} Q_{gi}^{d(s)} \\ Q_{gi}^{\max}, & \nu_i^{(s)} \leq \nu_{0i} - K_{Qci} Q_{gi}^{\max} \end{cases}$$

$$i = 1, \dots, n_g, s = 1, \dots, n_s \quad (36)$$

$$Q_{gi}^{\min} \leq Q_{gi}^{(s)} \leq Q_{gi}^{\max}, i = 1, \dots, n_g, s = 1, \dots, n_s \quad (37)$$

$$\nu_{0i}^{\min} \leq \nu_{0i} \leq \nu_{0i}^{\max}, i = 1, \dots, n_g \quad (38)$$

$$K_{Qci} \in \left\{ K_{Qci}^{(1)}, \dots, K_{Qci}^{(n_d)} \right\}, i = 1, \dots, n_g \quad (39)$$

The proposed droop control schemes apply to dispatchable distributed energy generation technologies such as combustion turbines, cogeneration, energy storage systems, microturbines, and reciprocating engines [29]. In this case, a commonly adopted model of the real (33) and reactive (37) power dispatch region is a box bounded by the lower and upper real and reactive power limits [20].

### C. Big-M Method

The mathematical programming formulation having the conditional choice constraints (32) and (36) is not directly in the format of MICP. In addition, although the discrete sets (35) and

(39) avoid the bilinear terms and retain the convexity of the continuous relaxation, they necessitate the introduction of big-M constraints in the model. Both of these aspects are described below.

1) *Real Power Droop*: The real power generation conditional choice-value in a given scenario (32) is modeled using two binary variables,  $\underline{\gamma}_i^{(s)}$  and  $\bar{\gamma}_i^{(s)}$ , as shown in (40). The sum of the binary variables is restricted to a maximum of one, as shown in (42), thus either one of the binary variables is one, or they are both zero. The setup together with (43) leads to three distinct cases:  $\underline{\gamma}_i^{(s)} = 1$  giving  $P_{gi}^{(s)} = P_{gi}^{\min}$ ,  $\bar{\gamma}_i^{(s)} = 1$  giving  $P_{gi}^{(s)} = P_{gi}^{\max}$ , and  $\underline{\gamma}_i^{(s)} = \bar{\gamma}_i^{(s)} = 0$  giving  $P_{gi}^{(s)} = P_{gi}^{d(s)}$ . When  $P_{gi}^{(s)} = P_{gi}^{d(s)}$ , the value of  $P_{gi}^{d(s)}$  will be related to the scenario frequency via the linear droop equation for the specific choice of the real power droop gain. This is modeled using the big-M constraints (44), where  $\eta_{Pi}^{(k,s)}$  is zero only when  $\underline{\gamma}_i^{(s)} = \bar{\gamma}_i^{(s)} = 0$  (i.e., the linear droop is used for generator- $i$  in scenario- $s$ ) and  $\alpha_i^{(k)} = 0$  (i.e., the  $k^{\text{th}}$  droop gain is chosen for generator- $i$ ), as given by the OR function (45). Eq (46) allows only one binary variable  $\alpha_i^{(k)}$  to be zero over  $k = 1, \dots, n_d$ , corresponding to the choice of the  $k^{\text{th}}$  droop  $K_{Pi}^{(k)}$ . Therefore  $K_{Pi}$  is given by (48), where only one of the  $K_{Pi}^{(k)}$  values survives the product. The values of the big-M parameters  $M_{Pi}^{(k)-}$  and  $M_{Pi}^{(k)+}$  in (44) are given in subsection III-D.

$$P_{gi}^{(s)} = \underline{\gamma}_i^{(s)} P_{gi}^{\min} + \bar{\gamma}_i^{(s)} P_{gi}^{\max} + P_{gi}^{d(s)}$$

$$i = 1, \dots, n_g, s = 1, \dots, n_s \quad (40)$$

$$\underline{\gamma}_i^{(s)} \in \{0, 1\}, \bar{\gamma}_i^{(s)} \in \{0, 1\} \quad (41)$$

$$\underline{\gamma}_i^{(s)} + \bar{\gamma}_i^{(s)} \leq 1, i = 1, \dots, n_g, s = 1, \dots, n_s \quad (42)$$

$$P_{gi}^{\min} \left( 1 - \underline{\gamma}_i^{(s)} - \bar{\gamma}_i^{(s)} \right) \leq P_{gi}^{d(s)} \leq P_{gi}^{\max} \left( 1 - \underline{\gamma}_i^{(s)} - \bar{\gamma}_i^{(s)} \right)$$

$$i = 1, \dots, n_g, s = 1, \dots, n_s \quad (43)$$

$$M_{Pi}^{(k)-} \eta_{Pi}^{(k,s)} \leq f^{(s)} - f_{0i} + K_{Pi}^{(k)} P_{gi}^{d(s)} \leq M_{Pi}^{(k)+} \eta_{Pi}^{(k,s)}$$

$$i = 1, \dots, n_g, k = 1, \dots, n_d, s = 1, \dots, n_s \quad (44)$$

$$\eta_{Pi}^{(k,s)} = \text{OR} \left( \underline{\gamma}_i^{(s)} + \bar{\gamma}_i^{(s)}, \alpha_i^{(k)} \right)$$

$$i = 1, \dots, n_g, k = 1, \dots, n_d, s = 1, \dots, n_s \quad (45)$$

$$\sum_{k=1}^{n_d} \alpha_i^{(k)} = n_d - 1, i = 1, \dots, n_g \quad (46)$$

$$\alpha_i^{(k)} \in \{0, 1\}, i = 1, \dots, n_g, k = 1, \dots, n_d \quad (47)$$

$$K_{Pi} = \sum_{k=1}^{n_d} K_{Pi}^{(k)} \left( 1 - \alpha_i^{(k)} \right), i = 1, \dots, n_g \quad (48)$$

Eqs. (49) and (50) define the frequency limits of the real power droop equation. Eq (49) ensures that the droop relation evaluated at minimum generation is less than the maximum allowed frequency, and (50) states that the droop equation at maximum generation is greater than the minimum allowed frequency. Eqs

(51) and (52) model the limits of the scenario frequency corresponding to  $P_{gi}^{\min}$  and  $P_{gi}^{\max}$ , as described in the first and last equations in (32). Consider for illustration (51). When  $\underline{\gamma}_i^{(s)} = 1$ , i.e., corresponding to  $P_{gi}^{(s)} = P_{gi}^{\min}$  as in (40), the left-hand side of (51) will be greater than or equal to zero as desired. However, when  $\underline{\gamma}_i^{(s)} = 0$ , meaning that  $P_{gi}^{(s)}$  is not at its minimum value, (51) reduces to (53), which is dominated by  $f^{(s)} \geq f^{\min}$  in (31) due to the constraint (49). Similar reasoning justifies the left-hand side of (52).

$$f_{0i} - K_{Pi}P_{gi}^{\min} \leq f^{\max} \quad (49)$$

$$\begin{aligned} f^{\min} &\leq f_{0i} - K_{Pi}P_{gi}^{\max} \\ i &= 1, \dots, n_g \end{aligned} \quad (50)$$

$$\begin{aligned} f^{(s)} - f_{0i} + K_{Pi}P_{gi}^{\min} &\geq (f^{\min} - f^{\max}) \left(1 - \underline{\gamma}_i^{(s)}\right) \\ i &= 1, \dots, n_g, \quad s = 1, \dots, n_s \end{aligned} \quad (51)$$

$$\begin{aligned} f^{(s)} - f_{0i} + K_{Pi}P_{gi}^{\max} &\leq (f^{\max} - f^{\min}) \left(1 - \overline{\gamma}_i^{(s)}\right) \\ i &= 1, \dots, n_g, \quad s = 1, \dots, n_s \end{aligned} \quad (52)$$

$$f^{(s)} \geq f^{\min} - (f^{\max} - f_{0i} + K_{Pi}P_{Gi}^{\min}) \quad (53)$$

2) *Reactive Power Droop*: Eqs. (54)–(66) are the direct counterparts of (40)–(52) for reactive power droop. The reactive power generation conditional-choice value for a given scenario, as defined by (36), is formulated by using two binary variables  $\underline{\lambda}_i^{(s)}$  and  $\overline{\lambda}_i^{(s)}$ , as in (54). The choice of the reactive power droop gain is again using the binary variable  $\beta_i^{(k)}$ , where the OR function (59) with inputs  $(\underline{\lambda}_i^{(s)} + \overline{\lambda}_i^{(s)})$  and  $\beta_i^{(k)}$  switches the reactive power droop relation on or off (58). The three conditions in (36) map to the big-M formulation constraints (58) and (65)–(66). The relations imposed on the binary variables allow only one of the equations in (58), (65), and (66) to effectively constrain the model for a given generator in a particular scenario.

$$\begin{aligned} Q_{gi}^{(s)} &= \underline{\lambda}_i^{(s)}Q_{gi}^{\min} + \overline{\lambda}_i^{(s)}Q_{gi}^{\max} + Q_{gi}^{d(s)} \\ i &= 1, \dots, n_g, \quad s = 1, \dots, n_s \end{aligned} \quad (54)$$

$$\underline{\lambda}_i^{(s)} \in \{0, 1\}, \quad \overline{\lambda}_i^{(s)} \in \{0, 1\} \quad (55)$$

$$\underline{\lambda}_i^{(s)} + \overline{\lambda}_i^{(s)} \leq 1, \quad i = 1, \dots, n_g, \quad s = 1, \dots, n_s \quad (56)$$

$$\begin{aligned} Q_{gi}^{\min} \left(1 - \underline{\lambda}_i^{(s)} - \overline{\lambda}_i^{(s)}\right) &\leq Q_{gi}^{d(s)} \leq Q_{gi}^{\max} \left(1 - \underline{\lambda}_i^{(s)} - \overline{\lambda}_i^{(s)}\right) \\ i &= 1, \dots, n_g, \quad s = 1, \dots, n_s \end{aligned} \quad (57)$$

$$\begin{aligned} M_{Qi}^{(k)-} \eta_{Qi}^{(k,s)} &\leq \nu_i^{(s)} - \nu_{0i} + K_{Qci}Q_{gi}^{d(s)} \leq M_{Qi}^{(k)+} \eta_{Qi}^{(k,s)} \\ i &= 1, \dots, n_g, \quad k = 1, \dots, n_d, \quad s = 1, \dots, n_s \end{aligned} \quad (58)$$

$$\begin{aligned} \eta_{Qi}^{(k,s)} &= \text{OR} \left( \underline{\lambda}_i^{(s)} + \overline{\lambda}_i^{(s)}, \beta_i^{(k)} \right) \\ i &= 1, \dots, n_g, \quad k = 1, \dots, n_d, \quad s = 1, \dots, n_s \end{aligned} \quad (59)$$

$$\sum_{k=1}^{n_d} \beta_i^{(k)} = n_d - 1, \quad i = 1, \dots, n_g \quad (60)$$

$$\beta_i^{(k)} \in \{0, 1\}, \quad i = 1, \dots, n_g, \quad k = 1, \dots, n_d \quad (61)$$

$$K_{Qci} = \sum_{k=1}^{n_d} K_{Qci}^{(k)} \left(1 - \beta_i^{(k)}\right), \quad i = 1, \dots, n_g \quad (62)$$

$$\nu_{0i} - K_{Qci}Q_{gi}^{\min} \leq \nu_i^{\max} \quad (63)$$

$$\begin{aligned} \nu_i^{\min} &\leq \nu_{0i} - K_{Qci}Q_{gi}^{\max} \\ i &= 1, \dots, n_g \end{aligned} \quad (64)$$

$$\begin{aligned} \nu_i^{(s)} - \nu_{0i} + K_{Qci}Q_{gi}^{\min} &\geq (\nu_i^{\min} - \nu_i^{\max}) \left(1 - \underline{\lambda}_i^{(s)}\right) \\ i &= 1, \dots, n_g, \quad s = 1, \dots, n_s \end{aligned} \quad (65)$$

$$\begin{aligned} \nu_i^{(s)} - \nu_{0i} + K_{Qci}Q_{gi}^{\max} &\leq (\nu_i^{\max} - \nu_i^{\min}) \left(1 - \overline{\lambda}_i^{(s)}\right) \\ i &= 1, \dots, n_g, \quad s = 1, \dots, n_s \end{aligned} \quad (66)$$

#### D. The OR Function Implementation and Big-M Parameters

The OR function in (45) has two inputs:  $(\underline{\gamma}_i^{(s)} + \overline{\gamma}_i^{(s)})$  which can be either zero or one, and the binary variable  $\alpha_i^{(k)}$ . Thus, the function can be equivalently written in terms of the linear constraints (67)–(70). A similar set holds for the second OR function in (59).

$$0 \leq \eta_{Pi}^{(k,s)} \leq 1 \quad (67)$$

$$\eta_{Pi}^{(k,s)} \geq \underline{\gamma}_i^{(s)} + \overline{\gamma}_i^{(s)} \quad (68)$$

$$\eta_{Pi}^{(k,s)} \geq \alpha_i^{(k)} \quad (69)$$

$$\begin{aligned} \eta_{Pi}^{(k,s)} &\leq \underline{\gamma}_i^{(s)} + \overline{\gamma}_i^{(s)} + \alpha_i^{(k)} \\ i &= 1, \dots, n_g, \quad k = 1, \dots, n_d, \quad s = 1, \dots, n_s \end{aligned} \quad (70)$$

The big-M parameter values in (44) and (58) should be large to the extent that they do not affect the optimal solution when the droop gains are not selected. However, setting them to an arbitrarily large value may result in ill-conditioning and affect the convergence of the search method. To determine the smallest possible values of the big-M parameters in (44), consider two cases. First, consider that when  $P_{gi}^{d(s)}$  is zero from (43), the expression within bounds reduces to  $f^{(s)} - f_{0i}$ , and the corresponding right-hand side (RHS) and left-hand side (LHS) limits are set to  $f^{\max} - f_{0i}^{\min}$  and  $f^{\min} - f_{0i}^{\max}$ , respectively. Second, consider that  $P_{gi}^{d(s)}$  is nonzero, and assume that the optimal setting of the real power droop gain is  $K_{Pi}^*$ , as shown in (71). Therefore, the value within limits in (44) is given by (72). Because  $K_{Pi}^*$  is initially unknown and  $0 \leq P_{Gi}^{\min} \leq P_{Gi}^{(s)} \leq P_{Gi}^{\max}$ , the big-M parameters can be set as in (73)–(74), where the discrete set of gains is assumed to be ordered  $(0 < K_{Pi}^{r(1)} < \dots < K_{Pi}^{(k)} < \dots < K_{Pi}^{(nd)})$  and the maximum droop gain  $K_{Pi}^{(nd)}$  is given by (2). Combining the expression of the big-M limits for the cases when  $P_{gi}^{d(s)}$  is zero and nonzero gives the desired

result in (75)–(76).

$$f^{(s)} - f_{0i} = -K_{P_i}^* P_{g_i}^{d(s)}, \quad i = 1, \dots, n_g, \quad s = 1, \dots, n_s \quad (71)$$

$$\Delta_{P_i}^{(k,s)} = f^{(s)} - f_{0i} + K_{P_i}^{(k)} P_{g_i}^{d(s)} = \left( K_{P_i}^{(k)} - K_{P_i}^* \right) P_{g_i}^{d(s)} \quad (72)$$

$i = 1, \dots, n_g, \quad k = 1, \dots, n_d, \quad s = 1, \dots, n_s$

$$\Delta_{P_i}^{(k)+} = \left( K_{P_i}^{(k)} - K_{P_i}^{(1)} \right) P_{g_i}^{\max} \leq K_{P_i}^{(n_d)} P_{g_i}^{\max} = f^{\max} - f^{\min} \quad (73)$$

$$\Delta_{P_i}^{(k)-} = \left( K_{P_i}^{(k)} - K_{P_i}^{(n_d)} \right) P_{g_i}^{\max} \geq -K_{P_i}^{(n_d)} P_{g_i}^{\max} = f^{\min} - f^{\max} \quad (74)$$

$$M_{P_i}^{(k)+} = f^{\max} - \min(f_{0i}^{\min}, f^{\min}) \quad (75)$$

$$M_{P_i}^{(k)-} = f^{\min} - \max(f_{0i}^{\max}, f^{\max}) \quad (76)$$

Furthermore, if  $0 \leq Q_{G_i}^{\min} \leq Q_{G_i}^{(s)} \leq Q_{G_i}^{\max}$ , the big-M parameters for reactive power droop gains are similarly given by (77)–(78).

$$M_{Q_i}^{(k)+} = \nu_i^{\max} - \min(\nu_{0i}^{\min}, \nu_i^{\min}) \quad (77)$$

$$M_{Q_i}^{(k)-} = \nu_i^{\min} - \max(\nu_{0i}^{\max}, \nu_i^{\max}) \quad (78)$$

### E. MICP Solution in Linear Droop Implementation

The desired MICP problem is given by (29)–(31), (33)–(34), (37)–(38), (40)–(52), and (54)–(66) with the OR function represented as in (67)–(70). Solving the MICP problem gives the following parameters for each distributed generator- $i$ :  $f_{0i}$ ,  $K_{P_i}$ ,  $\nu_{0i}$ , and  $K_{Q_{ci}}$ . Therefore, the corresponding linear droop equation for real power is given in (79). For reactive power droop, the equation is linear in terms of the squared voltage (80). For use in the regular linear droop implementation, (81) can be approximated by (82) with  $K_{Q_i}$  evaluated at one per-unit node voltage (82), as shown in the development below.

$$f = f_0 - K_{P_i} P_{g_i}, \quad i = 1, \dots, n_g \quad (79)$$

$$V_i^2 = V_{0i}^2 - K_{Q_{ci}} Q_{g_i}, \quad i = 1, \dots, n_g \quad (80)$$

$$(V_i - V_{0i})(V_i + V_{0i}) = -K_{Q_{ci}} Q_{g_i}, \quad i = 1, \dots, n_g \quad (81)$$

$$V_i \cong V_{0i} - K_{Q_i} Q_{g_i}, \quad i = 1, \dots, n_g \quad (82)$$

$$K_{Q_i} = \frac{K_{Q_{ci}}}{1 + V_{0i}} \quad (83)$$

## IV. NUMERICAL RESULTS

The MICP method for droop-controller design was in Matlab, and CPLEX was used for solving the MICP test instances [30]. The testing was carried out on five radial AC microgrids with 4, 9, 43, 84, and 136 buses operated in island mode. Table I shows the number of nodes  $n$ , the number of branches  $n_b$ , the number of distributed generators  $n_g$ , and the original reference for the network data. The number of buses includes the additional generation nodes for connecting the distributed generator

TABLE I  
TEST SYSTEM STATISTICS

$n$	4	9	43	84	136
$n_b$	3	8	42	83	135
$n_g$	3	3	5	8	8
ref.	[20]	[32]	[32]	[33]	[34]

impedance. Following [20], the MICP design considers three loading snapshots at high, medium, and low levels with equal probability values. Each generator's real and reactive power droop gain was allowed to vary in a discrete set of ten equally spaced values ( $n_d = 10$ ). The maximum value in the set is equal to the value from traditional droop control, i.e., (2) and (4). Thus, each set comprises ten droop gain values equally spaced between the maximum value divided by ten and the maximum droop gain value. The complete data sets that would allow replication of the results in the paper are available for download from [31]. Two MICP designs were computed for each system:

- MICP-F: The MICP design as described in Section III with the no-load frequency and no-load voltage fixed at their maximum value. The minimum limits in (34) and (38) are set equal to their maximum values, so the droop control design parameters are the real and reactive power droop gains ( $K_{P_i}, K_{Q_i}$ ). The MICP-F solutions only optimize the gains, as in the schemes described in subsection II-B.
- MICP-V: The MICP design as described in Section III with both the controller no-load setpoints ( $f_{0i}, \nu_{0i}$ ) and gains ( $K_{P_i}, K_{Q_i}$ ) as variable design parameters.

MICP-V, therefore, has more degrees of freedom as compared to MICP-F. The MICP designed controllers are contrasted with three different designs:

- Trad: The traditional linear droop scheme [3] as described in subsection II-A.
- Max-CB: The maximum cost-based linear droop scheme [20] as described in subsection II-B1.
- Av-CB: The average cost-based linear droop scheme [20] as described in subsection II-B2.

The controller design results for all methods and systems are available for download from [31]. Comparing the five droop control designs (MICP-F, MICP-V, Max-CB, Av-CB, Trad) requires simulating the microgrid using power flow under droop control. The Appendix introduces the Newton-Raphson based microgrid power flow method and its validation by comparison with the laboratory hardware implementation in [20].

Table II shows the average percentage increase in operational cost from MICP-F, MICP-V, and the above three methods compared to the cost from a centralized conic OPF solution (27)–(28). The conic OPF gives a global dispatch solution but does not rely upon droop control, making it an ideal benchmark for cost calculations. The average cost calculation in Table II is done over the three scenarios considered in the MICP designs and then under 100 load scenarios equally spaced between minimum and maximum loading and correspond to conforming changes in power injections. In the conforming case, loads in the microgrid are assumed to follow a similar rise and decline pattern during a day. Thus, in principle, the one hundred load scenarios

TABLE II  
PERCENTAGE INCREASE IN COST RELATIVE TO CENTRALIZED DISPATCH

$n_s$	$n$	4	9	43	84	136
3 (sample)	VIVS-F	4.07	3.13	2.08	2.86	2.06
	VIVS-V	0.00	0.00	0.20	0.06	0.03
	Max-CB	8.31	6.15	5.70	4.99	3.55
	Mean-CB	7.85	5.76	6.18	5.01	3.53
	Trad	24.94	19.03	17.74	13.93	10.25
100 (conforming)	VIVS-F	3.54	2.81	1.16	1.22	0.81
	VIVS-V	0.65	0.70	0.28	0.06	0.03
	Max-CB	7.54	6.01	4.37	3.39	2.28
	Mean-CB	7.09	5.66	4.71	3.30	2.20
	Trad	25.89	20.53	17.18	13.28	9.89
1000 (non-conforming)	VIVS-F	3.69	1.37	0.86	0.26	0.27
	VIVS-V	0.74	0.33	0.06	0.06	0.02
	Max-CB	7.70	4.30	2.37	1.06	0.53
	Mean-CB	7.22	3.86	3.07	1.18	0.59
	Trad	26.18	20.33	16.45	12.64	9.51

TABLE III  
PERCENTAGE OF NODES WITH VOLTAGE MAGNITUDE VIOLATIONS – AVERAGE & MAXIMUM OVER 100 CONFORMING SCENARIOS & 1000 NON-CONFORMING SCENARIOS

	$n$	4	9	43	84	136
Av. $n_s = 100$ (conforming)	MICP-F	0	0	0	0	0
	MICP-V	0	0	0	0	0
	Max-CB	0	0	0	2.30	0.88
	Av-CB	0	0	0	2.67	1.02
	Trad	0	0	2.87	11.38	2.41
Max $n_s = 100$ (conforming)	MICP-F	0	0	0	0	0
	MICP-V	0	0	0	0	0
	Max-CB	0	0	0	15.79	10.16
	Av-CB	0	0	0	17.11	10.16
	Trad	0	0	44.74	61.84	10.94
Av. $n_s = 1000$ (non-conforming)	MICP-F	0	0	0	0	0
	MICP-V	0	0	0	0	0
	Max-CB	0	0	0	0.01	0.01
	Av-CB	0	0	0	0.02	0.01
	Trad	0	0	0.04	0.28	0.01
Max $n_s = 1000$ (non-conforming)	MICP-F	0	0	0	0	0
	MICP-V	0	0	0	0	0
	Max-CB	0	0	0	13.16	10.16
	Av-CB	0	0	0	17.11	10.16
	Trad	0	0	44.74	61.84	10.94

can be arranged to depict load variation between minimum and maximum loading, and they also present out-of-sample analysis for the stochastic MICP solutions. Additionally, 1000 samples of non-conforming power injections, representing loads that can vary in an uncorrelated manner, are considered in the Monte-Carlo simulations. The results show that MICP-F and MICP-V are consistently better from an economic perspective for all test networks, an expected result given that their droop relationships are computed based on formal optimization theory. In particular, MICP-F gives lower cost than Max-CB, Mean-CB, and Trad as it allows optimizing the droop gains. On the other hand, MICP-V that additionally considers optimizing the no-load setpoints, yields costs slightly higher than centralized OPF.

Another advantage of the MICP solution is that it avoids voltage magnitude violations. Tables III, IV, and V show the extent of voltage magnitude violations experienced by the load nodes over the 100 conforming load scenarios and the 1000 non-conforming load snapshots, as measured by the percentage of load nodes with voltage magnitude violations (Table III),

TABLE IV  
MAXIMUM VOLTAGE MAGNITUDE VIOLATION [PU] AT A SINGLE NODE – AVERAGE & MAXIMUM OVER 100 CONFORMING SCENARIOS & 1000 NON-CONFORMING SCENARIOS

	$n$	4	9	43	84	136
Av. $n_s = 100$ (conforming)	MICP-F	0	0	0	0	0
	MICP-V	0	0	0	0	0
	Max-CB	0	0	0	1.84E-03	7.12E-04
	Av-CB	0	0	0	2.21E-03	9.01E-04
	Trad	0	0	1.43E-03	7.45E-03	3.16E-03
Max $n_s = 100$ (conforming)	MICP-F	0	0	0	0	0
	MICP-V	0	0	0	0	0
	Max-CB	0	0	0	1.59E-02	1.18E-02
	Av-CB	0	0	0	1.77E-02	1.35E-02
	Trad	0	0	1.53E-02	4.11E-02	2.34E-02
Av. $n_s = 1000$ (non-conforming)	MICP-F	0	0	0	0	0
	MICP-V	0	0	0	0	0
	Max-CB	0	0	0	1.52E-05	1.18E-05
	Av-CB	0	0	0	1.77E-05	1.35E-05
	Trad	0	0	1.53E-05	1.56E-04	2.34E-05
Max $n_s = 1000$ (non-conforming)	MICP-F	0	0	0	0	0
	MICP-V	0	0	0	0	0
	Max-CB	0	0	0	1.52E-02	1.18E-02
	Av-CB	0	0	0	1.77E-02	1.35E-02
	Trad	0	0	1.53E-02	4.11E-02	2.34E-02

TABLE V  
TOTAL VOLTAGE MAGNITUDE VIOLATION [PU] AT ALL NODES – AVERAGE & MAXIMUM OVER 100 CONFORMING SCENARIOS & 1000 NON-CONFORMING SCENARIOS

	$n$	4	9	43	84	136
Av. $n_s = 100$ (conforming)	MICP-F	0	0	0	0	0
	MICP-V	0	0	0	0	0
	Max-CB	0	0	0	1.17E-02	5.30E-03
	Av-CB	0	0	0	1.46E-02	7.18E-03
	Trad	0	0	5.48E-03	1.05E-01	3.13E-02
Max $n_s = 100$ (conforming)	MICP-F	0	0	0	0	0
	MICP-V	0	0	0	0	0
	Max-CB	0	0	0	1.21E-01	1.10E-01
	Av-CB	0	0	0	1.41E-01	1.31E-01
	Trad	0	0	8.16E-02	8.76E-01	2.62E-01
Av. $n_s = 1000$ (non-conforming)	MICP-F	0	0	0	0	0
	MICP-V	0	0	0	0	0
	Max-CB	0	0	0	1.12E-04	1.10E-04
	Av-CB	0	0	0	1.41E-04	1.31E-04
	Trad	0	0	8.16E-05	1.23E-03	2.62E-04
Max $n_s = 1000$ (non-conforming)	MICP-F	0	0	0	0	0
	MICP-V	0	0	0	0	0
	Max-CB	0	0	0	1.12E-01	1.10E-01
	Av-CB	0	0	0	1.41E-01	1.31E-01
	Trad	0	0	8.16E-02	8.76E-01	2.62E-01

the maximum voltage magnitude violation at a single node (Table IV), and the total voltage magnitude violation at all nodes (Table V). The results in these tables show that the droop schemes other than MICP give rise to voltage magnitude violations at a significant percentage of load buses, with worst-case violations in the traditional design method. This outcome is consistent with the fact that the droop designs other than MICP do not explicitly consider a microgrid network model. No frequency violations were encountered in any simulation when using the methods: MICP-F, MICP-V, Max-CB, Av-CB, and Trad.

Table VI shows the CPLEX computing time and relative optimality gap for solving the MICP test instances with default

TABLE VI  
CPLEX COMPUTING TIME [s] AND OPTIMALITY GAP [%]

	$n$	4	9	43	84	136
MICP-F	time [s]	4.6	2.8	404.1	900	900
	gap [%]	0.01	0.00	0.01	4.30	4.85
MICP-V	time [s]	1.5	1.8	822.4	900	900
	gap [%]	0.01	0.00	0.01	0.14	0.08

settings and a maximum allowed time of 15 minutes. The solution is computed on a MacBook Pro with a 2.9 GHz Intel Core i5 processor and 8 GB 2133 MHz memory. For MICP-V, the relative optimality gap is close to zero, and it is less than 5% for MICP-F.

### V. CONCLUSION

This paper presented a mixed-integer conic programming formulation for designing droop controllers in an islanded AC microgrid. The global optimality of the design can be ascertained for a predefined set of scenarios in a stochastic optimization framework; the formulation considers droop gain settings from a discrete set and the no-load frequency and voltage as continuous variables. Furthermore, the stochastic optimization problem allows distributed generators to operate in grid forming or grid feeding modes. The numerical results include comparisons with the classical droop method, the linear cost-based power-sharing schemes [20], and centralized generator dispatch [26]. Numerical comparative results show that the proposed approach is superior to the competing methods in both cost of operation and voltage magnitude violations and are pretty close to the centralized operation. The designs are also compatible with the existing hardware technology of linear droop implementations. Possible future research directions include solving the proposed formulation in a distributed way and considering three-phase unbalanced systems.

### APPENDIX

The microgrid Power Flow (PF) solution uses a polar formulation with  $n$  node voltage magnitudes and  $n$  node voltage angles [32]. The angle at an arbitrary bus is set to zero, giving rise to the following variables:  $n$  voltage magnitudes,  $(n - 1)$  voltage angles,  $n_g$  real power generation values,  $n_g$  reactive power generation values, and the system frequency. The total number of variables is, therefore,  $2n + 2n_g$ . The equations are  $n$  real power injection equations (84) and (86),  $n$  reactive power injection equations (85) and (87),  $n_g$  real power droop equations (88), and  $n_g$  reactive power droop equations (89). Therefore, the variables can be obtained from the nonlinear system (84)–(89) using the standard Newton-Raphson method. Upon convergence, the real or reactive power generation may exceed the prespecified generation limits. In this case, the generation value is held at the violated limit, and the corresponding droop relationship is dropped from the system of equations.

$$P_{gi} - f_P(V, \theta) = P_{di}, \quad i = 1, \dots, n_g \quad (84)$$

$$Q_{gi} - f_Q(V, \theta) = Q_{di}, \quad i = 1, \dots, n_g \quad (85)$$

TABLE VII  
POWER FLOW VERIFICATION: TRADITIONAL DROOP CONTROL

	Hardware PF [20]			Newton Raphson PF		
Loading	75%	50%	25%	75%	50%	25%
$P_{g1}$ [W]	750	500	250	752	501	250
$P_{g2}$ [W]	750	500	250	752	501	250
$P_{g3}$ [W]	750	500	250	752	501	250
$f$ [Hz]	49.50	50.00	50.50	49.50	50.00	50.50

TABLE VIII  
POWER FLOW VERIFICATION: MAX-CB DROOP CONTROL

	Hardware PF [20]			Newton Raphson PF		
Loading	75%	50%	25%	75%	50%	25%
$P_{g1}$ [W]	490	240	120	487	237	118
$P_{g2}$ [W]	770	380	190	769	374	187
$P_{g3}$ [W]	1000	880	440	1000	892	445
$f$ [Hz]	50.02	50.52	50.76	50.03	50.53	50.76

$$f_P(V, \theta) = -P_{di}, \quad i = n_g + 1, \dots, n \quad (86)$$

$$f_Q(V, \theta) = -Q_{di}, \quad i = n_g + 1, \dots, n \quad (87)$$

$$f + K_{P_i}^* P_{gi} = f_{0i}, \quad i = 1, \dots, n_g \quad (88)$$

$$V_i + K_{Q_i}^* Q_{gi} = V_{0i}, \quad i = 1, \dots, n_g \quad (89)$$

The implemented microgrid power flow was validated by comparing the results from a laboratory hardware implementation of a four-node network; one node corresponds to the load connection, and the remaining three are nodes of distributed generation connections. Ref. [20] reports the real power generation and microgrid frequency under three levels of loading as measured from the hardware implementation for traditional droop control (Table VII) and the maximum cost-based droop (Table VIII). The Tables also show the corresponding results from the Newton-Raphson power flow simulation, where the maximum discrepancy is within 2%. Thus, the above indicates the suitability of the Newton-Raphson power flow simulation for evaluating the microgrid performance under droop control.

### REFERENCES

- [1] J. M. Guerrero, J. C. Vasquez, J. Matas, L. G. de Vicuña, and M. Castilla, "Hierarchical control of droop-controlled AC and DC microgrids-A general approach toward standardization," *IEEE Trans. Ind. Electron.*, vol. 58, no. 1, pp. 158–172, Jan. 2011.
- [2] J.-O. Lee, Y.-S. Kim, and S.-I. Moon, "Novel supervisory control method for islanded droop-based AC/DC microgrids," *IEEE Trans. Power Syst.*, vol. 34, no. 3, pp. 2140–2151, May 2019.
- [3] Y. Sun, X. Hou, J. Yang, H. Han, M. Su, and J. M. Guerrero, "New perspectives on droop control in AC microgrid," *IEEE Trans. Ind. Electron.*, vol. 64, no. 7, pp. 5741–5745, Jul. 2017.
- [4] Y. Xu and H. Sun, "Distributed finite-time convergence control of an islanded low-voltage AC microgrid," *IEEE Trans. Power Syst.*, vol. 33, no. 3, pp. 2339–2348, May 2018.
- [5] J. S. Giraldo, J. A. Castrillon, J. C. López, M. J. Rider, and C. A. Castro, "Microgrids energy management using robust convex programming," *IEEE Trans. Smart Grid*, vol. 10, no. 4, pp. 4520–4530, Jul. 2019.
- [6] Q. Zhou, M. Shahidepour, Z. Li, and X. Xu, "Two-layer control scheme for maintaining the frequency and the optimal economic operation of hybrid AC/DC microgrids," *IEEE Trans. Power Syst.*, vol. 34, no. 1, pp. 64–75, Jan. 2019.
- [7] E. Espina, J. Llanos, C. Burgos-Mellado, R. Cárdenas-Dobson, M. Martínez-Gómez, and D. Sáez, "Distributed control strategies for microgrids: An overview," *IEEE Access*, vol. 8, pp. 193 412–193448, 2020.

- [8] Z. Zhang and M.-Y. Chow, "Convergence analysis of the incremental cost consensus algorithm under different communication network topologies in a smart grid," *IEEE Trans. Power Syst.*, vol. 27, no. 4, pp. 1761–1768, Nov. 2012.
- [9] S. Yang, S. Tan, and J.-X. Xu, "Consensus based approach for economic dispatch problem in a smart grid," *IEEE Trans. Power Syst.*, vol. 28, no. 4, pp. 4416–4426, Nov. 2013.
- [10] G. Binetti, A. Davoudi, F. L. Lewis, D. Naso, and B. Turchiano, "Distributed consensus-based economic dispatch with transmission losses," *IEEE Trans. Power Syst.*, vol. 29, no. 4, pp. 1711–1720, Jul. 2014.
- [11] G. Chen, F. L. Lewis, E. N. Feng, and Y. Song, "Distributed optimal active power control of multiple generation systems," *IEEE Trans. Ind. Electron.*, vol. 62, no. 11, pp. 7079–7090, Nov. 2015.
- [12] Q. Li, D. W. Gao, H. Zhang, Z. Wu, and F.-Y. Wang, "Consensus-based distributed economic dispatch control method in power systems," *IEEE Trans. Smart Grid*, vol. 10, no. 1, pp. 941–954, Jan. 2019.
- [13] Q. Zhou, M. Shahidehpour, Z. Li, L. Che, A. Alabdulwahab, and A. Abusorrah, "Compartmentalization strategy for the optimal economic operation of a hybrid AC/DC microgrid," *IEEE Trans. Power Syst.*, vol. 35, no. 2, pp. 1294–1304, Mar. 2020.
- [14] Q. Li *et al.*, "Parallel and distributed optimization method with constraint decomposition for energy management of microgrids," *IEEE Trans. Smart Grid*, vol. 12, no. 6, pp. 4627–4640, Nov. 2021.
- [15] F. Chen *et al.*, "Cost-based droop schemes for economic dispatch in islanded microgrids," *IEEE Trans. Smart Grid*, vol. 8, no. 1, pp. 63–74, Jan. 2017.
- [16] Q. Xu, J. Xiao, P. Wang, and C. Wen, "A decentralized control strategy for economic operation of autonomous AC, DC, and hybrid AC/DC microgrids," *IEEE Trans. Energy Conv.*, vol. 32, no. 4, pp. 1345–1355, Dec. 2017.
- [17] P. Yang, M. Yu, Q. Wu, P. Wang, Y. Xia, and W. Wei, "Decentralized economic operation control for hybrid AC/DC microgrid," *IEEE Trans. Sust. Energy*, vol. 11, no. 3, pp. 1898–1910, Jul. 2020.
- [18] I. U. Nutkani, P. C. Loh, and F. Blaabjerg, "Droop scheme with consideration of operating costs," *IEEE Trans. Power Electron.*, vol. 29, no. 3, pp. 1047–1052, Mar. 2014.
- [19] A. Elrayyah, F. Cingoz, and Y. Sozer, "Construction of nonlinear droop relations to optimize islanded microgrid operation," *IEEE Trans. Ind. Appl.*, vol. 51, no. 4, pp. 3404–3413, Jul./Aug. 2015.
- [20] I. U. Nutkani, P. C. Loh, P. Wang, and F. Blaabjerg, "Linear decentralized power sharing schemes for economic operation of AC microgrids," *IEEE Trans. Ind. Electron.*, vol. 63, no. 1, pp. 225–234, Jan. 2016.
- [21] R. A. Jabr and I. Džafić, "A compensation-based conic OPF for weakly meshed networks," *IEEE Trans. Power Syst.*, vol. 31, no. 5, pp. 4167–4168, Sep. 2016.
- [22] H. Xin, R. Zhao, L. Zhang, Z. Wang, K. P. Wong, and W. Wei, "A decentralized hierarchical control structure and self-optimizing control strategy for F-P type DGs in islanded microgrids," *IEEE Trans. Smart Grid*, vol. 7, no. 1, pp. 3–5, Jan. 2016.
- [23] L. Che, M. Shahidehpour, A. Alabdulwahab, and Y. Al-Turki, "Hierarchical coordination of a community microgrid with AC and DC microgrids," *IEEE Trans. Smart Grid*, vol. 6, no. 6, pp. 3042–3051, Nov. 2015.
- [24] S. Khongkhachat and S. Khomfoi, "Hierarchical control strategies in AC microgrids," in *Proc. 12th Int. Conf. Elect. Eng./Electron., Comput., Telecommun. Inf. Technol.*, 2015, pp. 1–6.
- [25] R. A. Jabr, "Mixed-integer convex optimization for DC microgrid droop control," *IEEE Trans. Power Syst.*, vol. 36, no. 6, pp. 5901–5908, Nov. 2021.
- [26] M. Farivar and S. H. Low, "Branch flow model: Relaxations and convexification-Part I," *IEEE Trans. Power Syst.*, vol. 28, no. 3, pp. 2554–2564, Aug. 2013.
- [27] R. A. Jabr, "Radial distribution load flow using conic programming," *IEEE Trans. Power Syst.*, vol. 21, no. 3, pp. 1458–1459, Aug. 2006.
- [28] D. K. Molzahn and I. A. Hiskens, "A Survey of Relaxations and Approximations of the Power Flow Equations," *Found. Trends Electric Energy Syst.*, vol. 4, no. 1/2, pp. 1–221, 2019.
- [29] U. S. Department of Energy - Office of Energy Efficiency and Renewable Energy, "Using distributed energy resources: A how-to guide for federal facility managers," May 2002. Accessed: Dec. 2, 2021. [Online]. Available: <https://www.nrel.gov/docs/fy02osti/31570.pdf>
- [30] IBM, "IBM ILOG CPLEX ver. 12.10 user's manual," IBM ILOG CPLEX division, Incline Village, NV, USA, 2019. [Online]. Available: <https://www.ibm.com/products>
- [31] R. A. Jabr, "Economic operation of droop-controlled AC microgrids - Data sets and designs," Accessed: Dec. 2, 2021. [Online]. Available: <https://www.dropbox.com/s/evqfyfa5h8h5saz/ACMG.zip?dl=0>
- [32] C. Li, S. K. Chaudhary, M. Savaghebi, J. C. Vasquez, and J. M. Guerrero, "Power flow analysis for low-voltage AC and DC microgrids considering droop control and virtual impedance," *IEEE Trans. Smart Grid*, vol. 8, no. 6, pp. 2754–2764, Nov. 2017.
- [33] C.-T. Su and C.-S. Lee, "Network reconfiguration of distribution systems using improved mixed-integer hybrid differential evolution," *IEEE Trans. Power Deliv.*, vol. 18, no. 3, pp. 1022–1027, Jul. 2003.
- [34] J. R. S. Mantovani, F. Casari, and R. A. Romero, "Reconfiguração de sistemas de distribuição radiais utilizando o critério de queda de tensão," *SBA: Controle Automação*, vol. 11, no. 2, pp. 150–159, Dec. 2000.



**Rabih A. Jabr** (Fellow, IEEE) was born in Lebanon. He received the B.E. degree in electrical engineering (with high distinction) from the American University of Beirut, Beirut, Lebanon, in 1997 and the Ph.D. degree in electrical engineering from Imperial College London, London, U.K., in 2000. He is currently a Professor with the Department of Electrical and Computer Engineering, American University of Beirut. His research interests include mathematical optimization techniques and power system analysis and computing.